Article

Synthesis and Magnetic Investigation of Ordered Mesoporous Two-Line Ferrihydrite

Harun Tysz, Elena Lorena Salaba, Claudia Weidenthaler, and Ferdi Schth

J. Am. Chem. Soc., **2008**, 130 (1), 280-287• DOI: 10.1021/ja075528j • Publication Date (Web): 12 December 2007

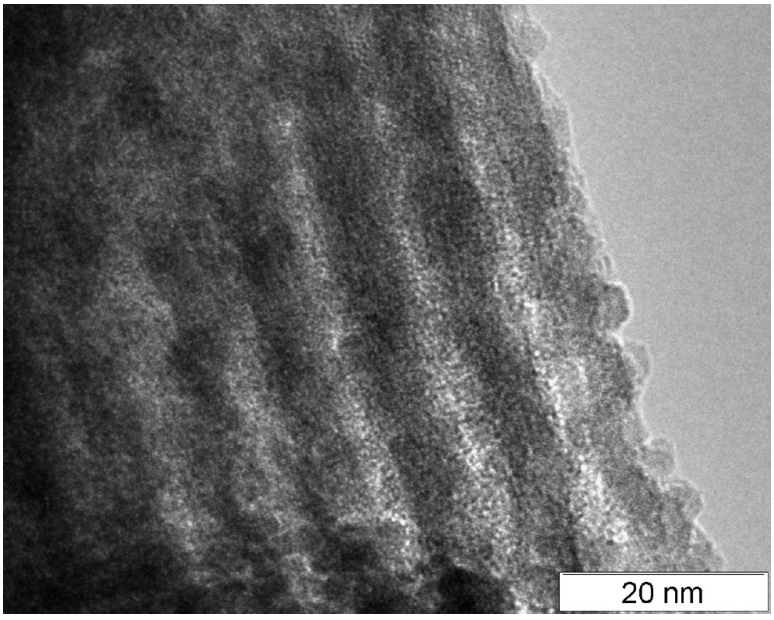

J|A|C|S
ARTICLES
Published on Web 12/12/2007

Synthesis and Magnetic Investigation of Ordered Mesoporous Two-Line Ferrihydrite

Harun Tüysüz, Elena Lorena Salabaş, Claudia Weidenthaler, and Ferdi Schüth*

Max-Planck Institut für Kohlenforschung, Kaiser-Wilhelm-Platz 1, D-45470 Mülheim an der Ruhr, Germany

Received August 9, 2007; E-mail: schueth@mpi-muelheim.mpg.de

Abstract: We report here for the first time on the synthesis and characterization of ordered mesoporous two-line ferrihydrite. Ordered mesoporous ferrihydrite has been prepared via the nanocasting route. Two types of ordered mesoporous silica, two-dimensional hexagonal SBA-15 and three-dimensional cubic KIT-6, were employed as hard templates. The magnetic behavior of ferrihydrite replicas with an average diameter of about 7 nm was investigated by direct current magnetometry. The temperature dependence of magnetization shows a superparamagnetic transition around 70 K. Field-induced changes in the low-field behavior of the magnetization were observed below 30 K. The results are explained assuming a spin-glass-like state of the surface spins. The 2D hexagonal two-line ferrihydrite showed very large coercivity up to 1.6 kOe at 5 K.

Introduction

Since the discovery of ordered mesoporous silica by Mobil scientists,[1] many reports have been published on different phases of ordered mesoporous silica, including hexagonal SBA-15[2] and cubic KIT-6.[3] SBA-15 has a two-dimensional well-ordered mesoporous hexagonal structure. SBA-15 is prepared under acidic conditions via cooperative assembly using a triblock copolymer as the structure-directing agent. KIT-6 has a three-dimensional cubic ordered mesoporous structure with topology similar to that of MCM-48.[4] The synthesis conditions for KIT-6 are rather similar to the ones for SBA-15. A triblock copolymer−butanol mixture is used as the structure-directing agent to synthesize KIT-6.

Following the cooperative assembly route, also non-silica materials such as TiO_2, ZrO_2, Al_2O_3, Nb_2O_5, Ta_2O_5, and WO_3 mesoporous materials were synthesized successfully.[5] Compared to the silicon alkoxides, the hydrolysis and polymerization of transition-metal alkoxides are more difficult to control. Therefore, the obtained metal oxides usually exhibit poor structural ordering and low thermal stability after removal of the surfactant templates. As an alternative to cooperative surfactant templating in solution, the nanocasting (hard templating) pathway was developed by Ryoo and co-workers.[6] According to this method, an ordered porous matrix acts as a nanoscopic mold, restricting through confinement the formation and growth of metal and metal oxide species. Due to the low decomposition temperature of the template, soft templating normally results in amorphous materials, whereas hard templating allows the formation of crystalline ordered mesoporous materials.[7,8] This nanocasting approach has been applied to produce different kinds of metal oxides, such as Co_3O_4,[9−11] Cr_2O_3,[12,13] CeO_2,[14] MgO,[15] α-Fe_2O_3,[12,16] γ-Fe_2O_3, and Fe_3O_4.[17]

Since we are interested in mesostructured materials showing collective magnetic properties, we are pursuing a program of mesostructuring different iron oxide-based materials. An interesting iron oxide phase, which is not even easily accessible as a bulk material, is ferrihydrite. The degree of crystallinity of ferrihydrite is variable and ranges from quasi-amorphous solids over poorly crystalline two-line ferrihydrite to a more ordered six-line ferrihydrite.

X-ray diffraction (XRD) patterns of two-line ferrihydrite are characterized by two broad peaks, while for six-line ferrihydrite six peaks are visible. This variety of crystallinities is associated with a poorly defined stoichiometry and a not well established atomic structure. The generally accepted chemical formulas for

(1) Kresge, C. T.; Leonowicz, M. E.; Roth, W. J.; Vartuli, J. C.; Beck, J. S. *Nature* **1992**, *359*, 710.
(2) Zhao, D.; Huo, Q.; Melosh, N.; Fredrickson, G. H.; Chmelka, B. F.; Stucky, G. D. *Science* **1998**, *279*, 548.
(3) Kleitz, F.; Choi, S. H.; Ryoo, R. *Chem. Commun.* **2003**, 2136.
(4) Beck, J. S.; Vartuli, J. C.; Roth, W. J.; Leonowicz, M. E.; Kresge, C. T.; Schmitt, K. D.; Chu, T. W.; Olson, D. H.; Sheppard, E. W.; McCullen, S. B.; Higgens, J. B.; Schlenker, J. L. *J. Am. Chem. Soc.* **1992**, *114*, 10834.
(5) Yang, P.; Zhao, D.; Margolese, D. I.; Chmelka, B. F.; Stucky, G. D. *Nature* **1998**, *396*, 152.
(6) Ryoo, R.; Joo, S. H.; Jun, S. *J. Phys. Chem. B* **1999**, *103*, 7743.
(7) Lu, A. H.; Schüth, F. *Adv. Mater.* **2006**, *18*, 1793.
(8) Yang, H.; Zhao, D. *J. Mater. Chem.* **2005**, *15*, 1217.
(9) Tian, B. Z.; Lui, X.; Solovyov, L.; Liu, Z.; Yang, H.; Zhang, Z.; Xie, S.; Zhang, F.; Tu, B; Yu, C.; Terasaki, O.; Zhao, D. *J. Am. Chem. Soc.* **2004**, *126*, 865.
(10) Wang, Y.; Yang, C. M.; Schmidt, W.; Spliethoff, B.; Bill, E.; Schüth, F. *Adv. Mater.* **2005**, *17*, 53.
(11) Rumplecker, A.; Kleitz, F.; Salabas, E. L.; Schüth, F. *Chem. Mater.* **2007**, *19*, 485.
(12) Tian, B.; Lui, X.; Yang, H.; Xie, S.; Yu, C.; Tu, B.; Zhao, D. *Adv. Mater.* **2003**, *15*, 1370.
(13) Jiao, K.; Zhang, B.; Yue, B9.; Ren, Y.; Liu, S.; Yan, S.; Dickinson, C.; Zhou, W.; He, H. *Chem. Commun.* **2005**, 5618.
(14) Laha, S.; Ryoo, R. *Chem. Commun.* **2003**, 2138.
(15) Roggenbuck, J.; Tiemann, M. *J. Am. Chem. Soc.* **2005**, *127*, 1096.
(16) Jiao, F.; Harrison, A.; Jumas, J. C.; Chadwick, A. V.; Kockelmann, W.; Bruce, P. G. *J. Am. Chem. Soc.* **2006**, *128*, 5468.
(17) Jiao, F.; Jumas, J. C.; Womes, M.; Chadwick, A. V.; Harrison, A.; Bruce, P. G. *J. Am. Chem. Soc.* **2006**, *128*, 12905.

10.1021/ja075528j CCC: $40.75

ferrihydrite are $Fe_5HO_8 \cdot 4H_2O$ and $5Fe_2O_3 \cdot 9H_2O$.[18,19] Regarding the crystal structure, it is believed that it corresponds to that of hematite.[20] It was proposed that the Fe^{3+} ions are octahedrally coordinated within a hexagonal unit cell, whereas the Fe^{3+} ions located on the surface (about 30%) have a tetrahedral coordination.[21] This lower coordination number for the Fe^{3+} surface ions can lead to very interesting properties, which can be exploited, for example, in the fields of catalysis and nanomagnetism. The Fe^{3+} ions in the bulk are coordinated by three O atoms and three OH groups with a $Fe^{3+}-Fe^{3+}$ separation of 3.01 Å. Detailed structure analysis of ferrihydrite was reported recently by Michel et al.[22,23]

Jansen et al.[24] performed neutron diffraction studies of six-line ferrihydrite and confirmed the model of a superposition of two components as described by Drits et al.[25] The crystal structure can be described best as the sum of a defect-free phase (space group $P\bar{3}1c$) and a defective phase ($P3$). The neutron diffraction data clearly revealed an ordered antiferromagnetic (AFM) state of ferrihydrite.

Magnetic properties of AFM nanoparticles are of great interest since these particles display a weak ferromagnetism at low temperatures and superparamagnetic behavior. Néel attributed this net magnetic moment per particle to the existence of uncompensated surface spins.[26] In the case of small AFM particles, the uncompensated spins arise mainly from the lower coordination of surface atoms and usually dominate the net magnetic response of AFM nanoparticles. Recently, the uncompensated spins have attracted a lot of interest, as their understanding appears to be of major importance in exchange-biased systems.[27,28] It has been proposed that nanostructured AFM materials may be used to stabilize the magnetization direction of ferromagnetic particles in magnetic recording media.[29] The nanocasting route provides great opportunities to synthesize, at will, complex magnetic systems with new magnetic properties. Novel hard magnetic materials consisting of interpenetrating composites of antiferomagnetic and ferromagnetic nanoparticles can be created.[30] Mesoporous nanoferryhidrite is a first step toward such systems, because it can be used as a template for building up 3D nanoscale magnetic heterostructures, which would be filled within a second, different magnetic material. The resulting composites would have tunable size and composition of the individual components of the heterostructure and could be used for exchange-bias applications.

Neutron studies performed by Seehra et al.[31] show that the ferrihydrite orders antiferromagnetically with a Néel temperature around 350 K. The magnetic properties of ferrihydrite have also been investigated by many groups using Mössbauer spectroscopy.[32] For ferrihydrite nanoparticles, a superparamagnetic transition in the range 60−100 K was observed, along with an average magnetic moment of 240 μ_B per particle in the case of particles with a diameter of 4 nm.[31]

In general, no noticeable differences have been observed between nanostructure and mesoporous ferrihydrite systems. The interesting magnetic properties compared to bulk arise from the finite size and surface effects.

In this paper, we show that the nanocasting route allows us to successfully synthesize hexagonal and cubic ordered mesoporous two-line ferrihydrite nanostructures. A complex magnetic behavior, mainly related to the surface effects, was observed. The low-temperature magnetometry measurements revealed an ordering temperature of around 70 K and a magnetic moment of about 295 μ_B per particle, resulting from the uncompensated Fe^{3+} spins. At low temperatures (below 30 K), a spin-glass-like state of the surface spins was identified.

Experimental Section

Nanostructured 2D hexagonal and 3D cubic two-line ferrihydrite (in the following labeled 2D- and 3D-ferrihydrite) were prepared using SBA-15 and KIT-6 as hard templates, which were synthesized according to literature.[3,34] In a typical synthesis of ordered mesoporous ferrihydrite, 5 mL of 0.8 M $Fe(NO_3)_3 \cdot 9H_2O$ (98%, Aldrich) in ethanol was added to 0.5 g of SBA-15 or KIT-6 and stirred at room temperature for 1 h. The ethanol was evaporated at 50 °C. The sample was then calcined at 200 °C and re-impregnated under the same conditions, followed by calcination at 200 °C for 6 h. The loading of ferrihydrite in the composite thus reached 50 wt %. The silica template was then removed using 2 M NaOH aqueous solution, followed by washing with water several times and then drying at 50 °C. The amount of silica in the ferrihydrite was adjusted with the treatment time of NaOH solution. We have varied several synthesis parameters (like calcination temperature, loading amount) in order to produce well-ordered samples. One of the most important parameters in creating ordered mesoporous materials via hard templating is the loading amount of the precursor. For the case of ferrihydrite, in order to create ordered structures, the template needs to be impregnated at least twice. At 250 °C, the ferrihydrite phase is obtained, but at 300 °C, the formation of hematite is observed. The procedure reported is the optimized synthesis.

The infrared (IR) spectra of samples were collected on a Magna-IR 750 Nicolet FTIR spectrometer using KBr tablets. The XRD patterns collected at room temperature were recorded on a Stoe theta/theta diffractometer in Bragg−Brentano geometry (Cu Kα radiation). The X-ray powder patterns collected *in situ* in the temperature range between room temperature and 900 °C were recorded on a Stoe STADI P transmission diffractometer in Debye−Scherrer geometry (Mo $K\alpha_1$, 0.70930 Å) with a primary monochromator and an image plate detector. For the *in situ* high-temperature experiments, a capillary furnace was attached to the diffractometer. Data were collected in the range between 7 and 50° 2θ. For the measurements, the samples were filled into 0.5-mm-diameter quartz glass capillaries. Heating rates of 10 °C min^{-1} were applied. The measured patterns were evaluated qualitatively by comparison with entries from the PDF-2 powder pattern database or with calculated patterns using literature structure data.

(18) Towe, K. M.; Bradley, W. F. *J. Colloid Interface Sci.* **1967**, *24*, 384.
(19) Cornell R. M.; Schwertman, U. *The Iron Oxides Structure, Properties, Reactions, Occurrences and Uses*, 2nd ed.; Wiley-VCH: Weinheim, 2003.
(20) Jambor, J.; Dutrizac, J. *Chem. Rev.* **1998**, *98*, 2549.
(21) Zhao, J.; Huggins, F. E.; Feng, Z.; Huffman, G. P. *Clays Clay Miner.* **1994**, *42*, 737.
(22) Michel, F. M.; Ehm, L.; Liu, G.; Han, W. Q.; Antao, S. M.; Chupas, P. J.; Lee, P. L.; Knorr, K.; Eulert, H.; Kim, J.; Grey, C. P.; Celestian, A. J.; Gillow, J.; Schoonen, M. A. A.; Strongin, D. R.; Parise, J. B. *Chem. Mater.* **2007**, *19*, 1489.
(23) Michel, F. M.; Ehm, L.; Antao, S. M.; Lee, P. L.; Chupas, P. J.; Liu, G.; Strongin, D. R.; Schoonen, M. A. A.; Phillips, B. L.; Parise, J. B. *Science* **2007**, *316*, 1726.
(24) Jansen, E.; Kyek, A.; Schafer, W. *Appl. Phys. A−Mater. Sci. Processing* **2002**, *74*, 1004.
(25) Drits, V. A.; Sakharov, B. A.; Salyn, A.; Manceau, A. *Clay Miner.* **1993**, *28*, 185.
(26) Néel, L. *Low Temperature Physics*; Gordon and Breach: New York, 1962.
(27) Salabas, E. L.; Rumplecker, A.; Kleitz, F.; Radu, F.; Schüth, F. *Nano Lett.* **2006**, *6*, 2977.
(28) Ohldag, H.; Scholl, A.; Nolting, F.; Arenholz, E.; Maat, S.; Young, A. T.; Carey, M.; Stöhr, J. *Phsy. Rev. Lett.* **2003**, *91*, 17203.
(29) Skumryev, V.; Stoyanov, S.; Zhang, Y.; Hadjipanayis, G.; Givord, D.; Nogues, J. *Nature* **2003**, *433*, 850.
(30) Lu, A. H.; Salabas, E. L.; Schüth, F. *Angew. Chem., Int. Ed.* **2007**, *46*, 1222.
(31) Seehra, M. S.; Babu, V. S.; Manivannan, A.; Lynn, J. W. *Phys. Rev. B* **2000**, *61*, 3513.
(32) Madsen, M. B.; Mørup, S.; Koch, C. J. W. *Hyperfine Int.* **1986**, *27*, 329.
(33) Ref deleted in proof.
(34) Choi, M.; Heo, W.; Kleitz, F.; Ryoo, R. *Chem. Commun.* **2003**, 1340.

Nitrogen adsorption isotherms were measured with an ASAP 2010 adsorption analyzer (Micromeritics) at liquid nitrogen temperature. Prior to the measurements, the samples were degassed at 100 °C for 10 h. Total pore volumes were determined using the adsorbed volume at a relative pressure of 0.97. Brunauer−Emmett−Teller (BET) surface area was estimated from the relative pressure range between 0.06 and 0.2. Pore size distribution (PSD) curves were calculated by the Barrett−Joyner−Halenda (BJH) method from the adsorption branch. Transmission electron microscopy (TEM) images of samples were obtained with a HF 2000 microscope (Hitachi) equipped with a cold-field emission gun. The acceleration voltage was 200 kV. Samples were prepared on lacey carbon grids. The thermal phase transformation of ferrihydrite was investigated using a Netzsch STA 449C thermal analyzer. The measurement was performed in a flow of air at a heating rate of 5 K/min.

The magnetic properties were investigated by means of magnetization measurements obtained using a superconducting quantum interference device (SQUID) magnetometer in the 2−280 K temperature range, with the applied fields up to 50 kOe. The samples were measured in powder form in a plastic capsule. The data presented here were corrected for the background signal from the sample holder with $\chi = M/H = -1.29 \times 10^{-8}$ emu/Oe.

Results and Discussion

The structure and crystallinity of the ferrihydrite samples were studied by XRD methods. The low-angle XRD pattern of template-free mesoporous 3D-ferrihydrite, nanocasted from KIT-6, is shown in Figure 1A. The diffraction pattern indicates an ordered mesoporous structure. The pattern exhibits only two broad reflections, which are assigned to the (211) and (220) reflections characteristic for the 3D cubic structure with $Ia\bar{3}d$ symmetry. These reflections alone would not be sufficient for clear structural assignment; however, due to the templating from KIT-6, the $Ia\bar{3}d$ structure is highly probable. From the (211) reflection, the unit cell parameter (a_0) was determined to be 22.7 nm. The wide-angle X-ray pattern ($2\theta = 15-70$) of mesoporous 3D-ferrihydrite is shown in Figure 1B. The two very broad reflections appearing at *d*-values of 2.6 Å (110) and 1.5 Å (300) are known to represent poorly crystalline two-line ferrihydrite.

The transformation of bulk ferrihydrite at higher temperatures into α-Fe_2O_3 has been the topic of several publications.[21,35,36,37] Depending on the use of organic reductants, one or two exothermic reactions take place during the transformation of six-line ferrihydrite into hematite.[36] Eggleton and Fitzpatrick discuss two transformations for two-line ferrihydrite between 340 and 355 °C and at 449 °C.[38] For six-line ferrihydrite, a transformation at 482 °C was observed. Already at about 310 °C, the peak at 2.52 Å for the six-line ferrihydrite sharpens and new reflections appear. At 400 °C, a mixture of maghemite and hematite six-line ferrihydrite is present, whereas at 500 °C, only hematite can be observed. For comparison with bulk two-line ferrihydrite, the temperature behavior of mesoporous two-line ferrihydrite was investigated by means of *in situ* powder diffraction studies. During the increase of temperature, the broad reflections at *d*-values of 2.5 and 1.5 Å known for two-line ferrihydrite start to get sharper (Figure 2A). The assignment of the reflections measured below 600 °C is difficult since both maghemite and ferrihydrite have reflections at almost the same

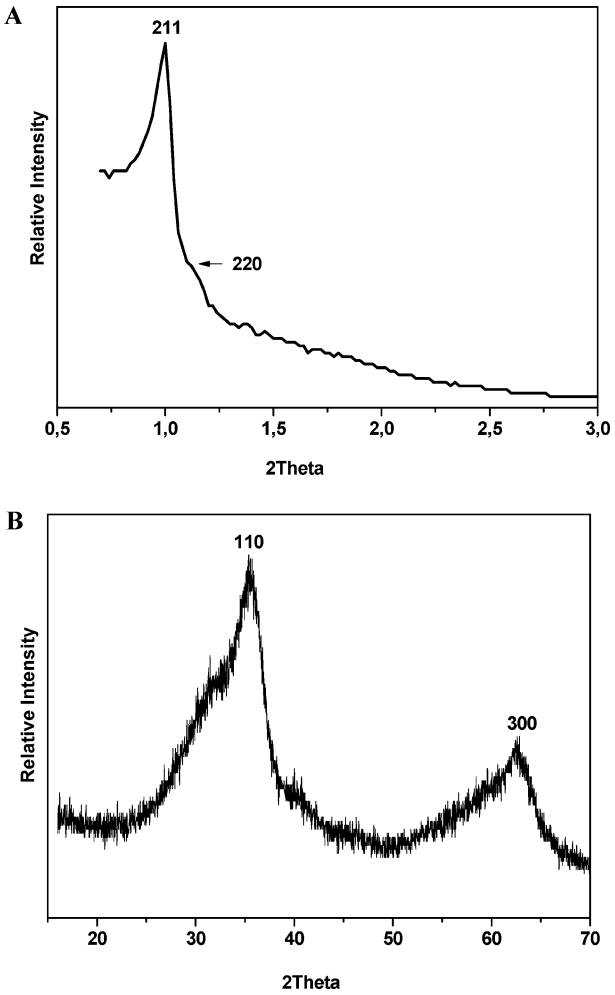

Figure 1. (A) Low- and (B) wide-angle XRD patterns of mesoporous cubic ferrihydrite.

d-values. A transformation of two-line ferrihydrite first to maghemite cannot be excluded. The pattern collected at 650 °C is significantly different, and the very narrow reflections belong exclusively to hematite.

Textural parameters of ferrihydrite were investigated by nitrogen physisorption. Figure 3 shows the nitrogen adsorption−desorption isotherm and the pore size distribution for cubic ordered mesoporous 3D-ferrrihydrite. The isotherm is of type IV and has the typical hysteresis loop of mesoporous materials or metal oxides prepared by the hard-templating method. The 3D-ferrihydrite has a BET surface area of 222 $m^2\ g^{-1}$ and a pore volume of 0.54 $cm^3\ g^{-1}$, which are remarkably high for iron oxides. The peak of the pore size distribution is centered at 5.1 nm (Figure 3B).

A representative TEM image of 3D-ferrihydrite is displayed in Figure 4; lower magnification survey images are included in the Supporting Information. The mesoporous structure is well ordered and in accordance with the $Ia\bar{3}d$ symmetry, like the cubic KIT-6 template. The mesoporous material is rather homogeneous, and no bulk phase of ferrihydrite has been identified in the TEM measurements. The average particle size obtained from measurements on different particles is 7 ± 1 nm. The ferrihydrite nanoparticles are uniform with regard to size and

(35) Mazzetti, L.; Thistlethwaite, J. *Raman Spectrosc*. **2002**, *33*, 104.
(36) Campbell, A. S.; Schwertman, U.; Stanjek, H.; Friede, J.; Kyek, A.; Campbell, P. A. *Langmuir* **2002**, *18*, 7804.
(37) Cudennec, Y.; Lecerf, A. *J. Solid State Chem.* **2006**, *179*, 716.
(38) Eggleton, R. A.; Fitzpatrick, R. W. *Clay Miner*. **1988**, *36*, 111.

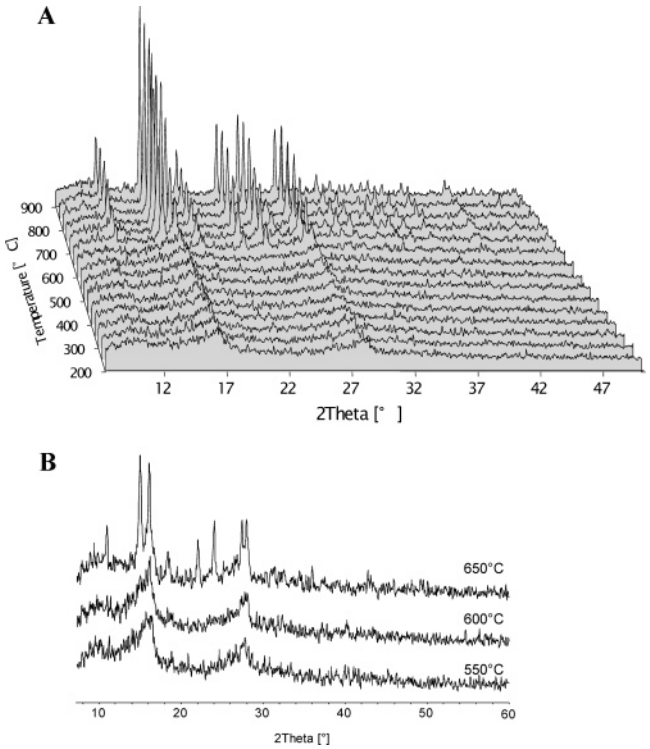

Figure 2. X-ray powder patterns collected *in situ* in the temperature ranges (A) 200−900 °C and (B) 550−650 °C.

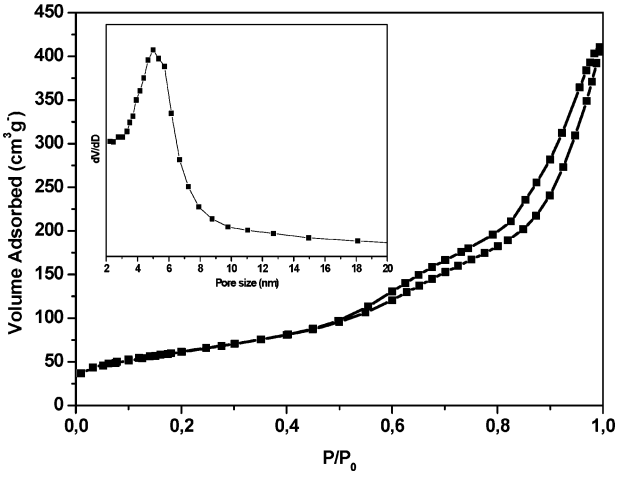

Figure 3. Nitrogen adsorption−desorption isotherms and (inset) pore size distribution for cubic ordered mesoporous ferrrihydrite.

shape, and TEM investigations indicate that ferrihydrite was successfully nanocasted from the KIT-6 template.

The influence of a small amount of silicon on the two-line ferrihydrite structure is considered next, since silicon could be left in the material due to the templating from the KIT-6 silica. From the energy-dispersive X-ray (EDX) analysis, we know that there is about 2% of silica still present in our sample after template removal. The presence of silica is visible in the differential thermal analysis (DTA) plot, where a shift of the temperature at which ferrihydrite converts to hematite was observed. Figure 5 shows the DTA plot of 3D-ferrihydrite. In case of pure ferrihydrite, the thermal transformation to hematite takes place at around 340 °C. As is shown in Figure 5, a weak exothermic peak around 790 °C was measured, which indicates that the presence of silica stabilizes the ferrihydrite and leads

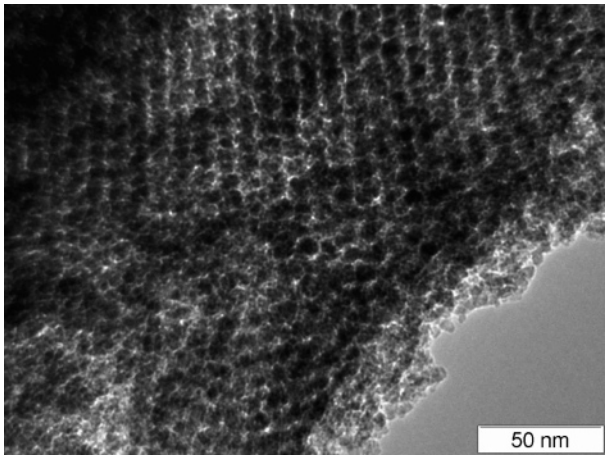

Figure 4. TEM image for mesoporous 3D-ferrihydrite.

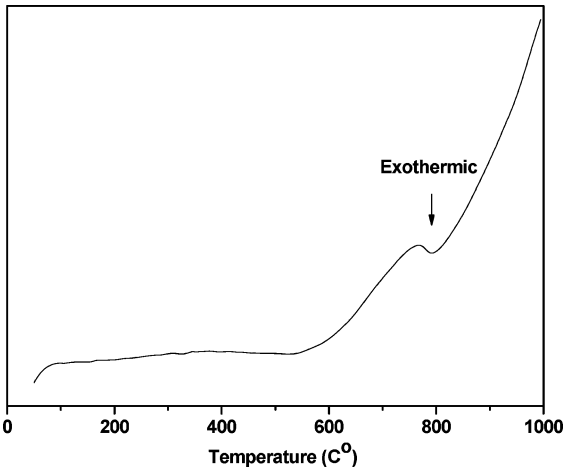

Figure 5. DTA curve of 3D-ferrihydrite.

to an increase in the transition temperature to hematite. The effect of different amounts of the silica on the transformation of the ferrihydrite was also investigated. In all cases, the transformation of silica-doped ferrihydrite to hematite occurs at higher temperatures compared to that of pure ferrihydrite, but no systematic dependence on the silicon content has been observed. It seems that even a small amount of silica has an important effect on the structural properties of ferrihydrite, a phenomenon also known from impurities in other oxides. One possible reason can be the large affinity of Si for the Fe−OH functional groups of iron. The transformation of ferrihydrite to hematite by dry heating requires a combination of dehydration/dehydroxylation and rearrangement processes, leading to a gradual structural ordering within the ferrihydrite particles toward the hematite structure. Ferrihydrite does not show a dehydroxylation peak. Similar effects were observed in other ferrihydrite systems. For example, higher temperatures are required for the thermal conversion of ferrihydrite to hematite when the ferrihydrite contains foreign elements such as Si, P, and Al. Campbell et al. observed in DTA measurements that increasing the Si (Si + Fe) ratio from 0 to 0.134 in two-line ferrihyrite caused the exothermic peak to shift from 340 to 740 °C.[36]

Studies on silica-doped ferrihydrite samples by Seehra et al.[39] showed that the presence of Si leads to an increase in

(39) Seehra, M. S.; Roy, P.; Raman, A.; Manivannan, A. *Solid State Commun.* **2004**, *130*, 597.

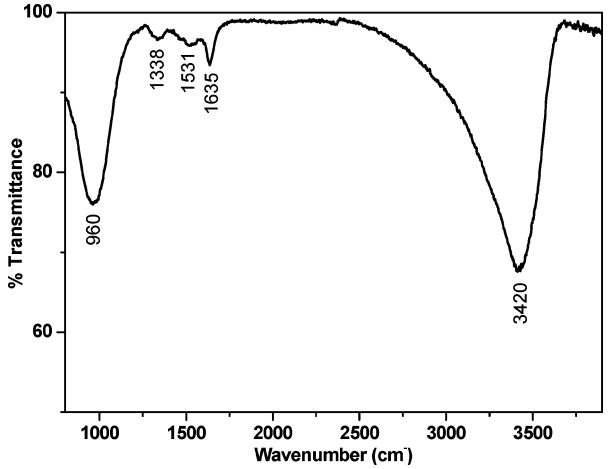

Figure 6. FTIR spectrum of 3D-ferrihydrite.

noncrystallinity and appearance of new modes in the IR spectra. The IR spectrum of 3D-ferrihydrite in the range 800−4000 cm^{-1} is shown in Figure 6, where five bands were identified. The absorption band at 3400 cm^{-1} can be attributed to OH groups. In general, the bands at 1338, 1531, and 1635 cm^{-1} are assigned to Fe−OH, Fe−O, and H_2O, respectively. The origin of the band at 960 cm^{-1} can be related to the presence of a tiny amount of silica. It was reported that the synthetic ferrihydrite does not show any band between 900 and 1000 cm^{-1}. In our case, the band at 960 cm^{-1} can be an identification of the Si−O−Fe groups. In the case of fully polymerized silica, Si−O stretching appears around 1100 cm^{-1}. Silixone linkages to heteroatoms or in defects typically appear at lower wavenumbers.[30] We therefore assign this band to Si−O−Fe groups formed by reaction of silanol groups with the Fe−OH functional groups of the surface, thereby forming Si−O−Fe bonds.

The influence of the silica on the formation of two-line ferrihydrite was underlined also by another experimental observation. Ferrihydrite is usually synthesized by rapid hydrolysis of a Fe(III) salt solution at about neutral pH. As we have shown here, ferrihydrite can be produced via the hydrothermal pathway using a silica template. If the precursor $Fe(NO_3)_3{\cdot}9H_2O$ is treated under the same conditions as in the nanocasting process, i.e., at 200 °C for 6 h, in the absence of silica, hematite is formed rather than ferrihydrite.

Though the nanocasting of such a transition iron oxide is interesting in itself, the main focus of our work is the production of nanostructured materials with interesting magnetic properties. We will first discuss the direct current magnetometry data of cubic ordered mesoporous 3D-ferrrihydrite. The temperature dependence (2−280 K) of the zero-field-cooled (ZFC) and field-cooled (FC) magnetization curves is shown in Figure 7. The ZFC curve was obtained by cooling the sample in zero field from room temperature to 2 K and then measuring the magnetization while increasing temperatures stepwise in a field of 100 Oe. In the FC experiments, the sample was cooled from room temperature to 2 K in a magnetic field of 50 kOe. The sample magnetization was then recorded in the same small applied magnetic field as the temperature was increased. These curves suggest the presence of superparamagnetic behavior of the nanoparticles with a characteristic blocking temperature, T_B = 70 K. Above the blocking temperature, the magnetization decreases due to the randomized effects induced by the k_BT,

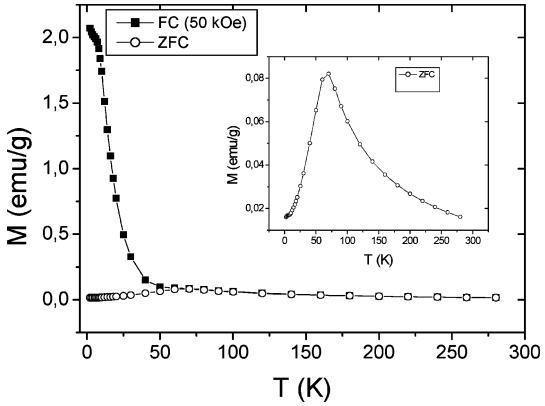

Figure 7. Temperature variation of the magnetization, measured in 100 Oe, for the zero-field-cooled (ZFC, ○) and field-cooled (FC, ■) cases. (Inset) A zoom-in of the ZFC curve is shown.

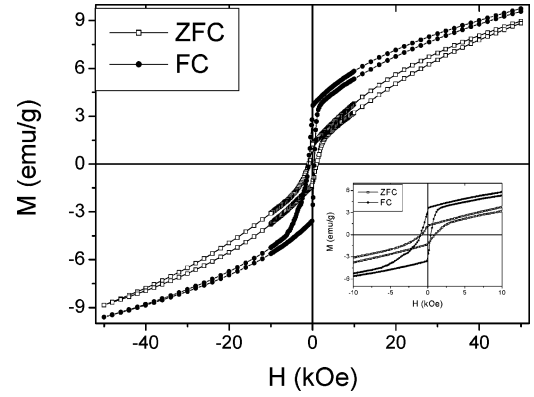

Figure 8. Zero-field-cooled (□) and field-cooled (●) hysteresis loops measured at 5 K up to ±50 kOe. (Inset) The low-field region is shown.

and the ZFC and FC curves overlap. Very large irreversibility (difference between ZFC and FC magnetization curves) was observed at low temperatures, below the blocking temperature. This indicates an induced preferential orientation of the particle moments along the applied field. By assuming a system of noninteracting single-domain particles, the blocking temperature can be used to estimate the effective magnetic anisotropy according to an expression which holds only for the measurement time window of the SQUID magnetometry (about 100 s): $K_{eff}V = 25k_BT_B$, where k_B is the Boltzmann constant and V is the volume of the particle. On the basis of the TEM investigations, we assume an average diameter of about 7 nm. Using this assumption, we obtain an effective anisotropy value of 1.34×10^5 J m^{-3}, which is within the wide range of the reported bulk value for ferrihydrite (0.3×10^5−6.1×10^5 J m^{-3}).[40]

In Figure 8, ZFC and FC magnetization curves as a function of magnetic field, measured at 5 K, are shown. The ZFC hysteresis clearly shows the ferromagnetic behavior of the ferrihydrite nanoparticles, where a coercivity of about 900 Oe and a remanence magnetization of 1.3 emu g^{-1} were measured. As a perfectly compensated antiferromagnet does not show hysteresis, we interpret the observed behavior as resulting from two contributions to the magnetization: a saturating ferromagnetic-like component coming from the surface spins and a field-linear AFM contribution coming from the core spins. The AFM

(40) Duarte, E. L.; Itri, R.; Lima, E., Jr.; Baptista, M. S.; Berquó, T. S.; Goya, G. T. *Nanotechnology* **2006**, *17*, 5549.

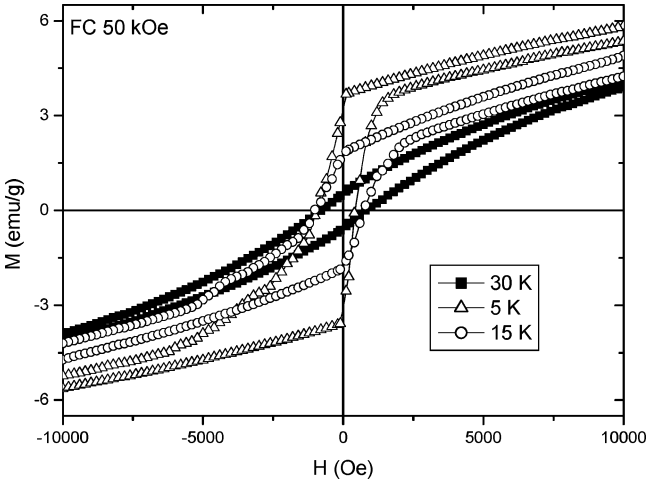

Figure 9. Low-field region of the field-cooled magnetization curves at 5 (△), 15 (○), and 30 K (■). The influence of the temperature on the shape of the hysteresis loops is striking.

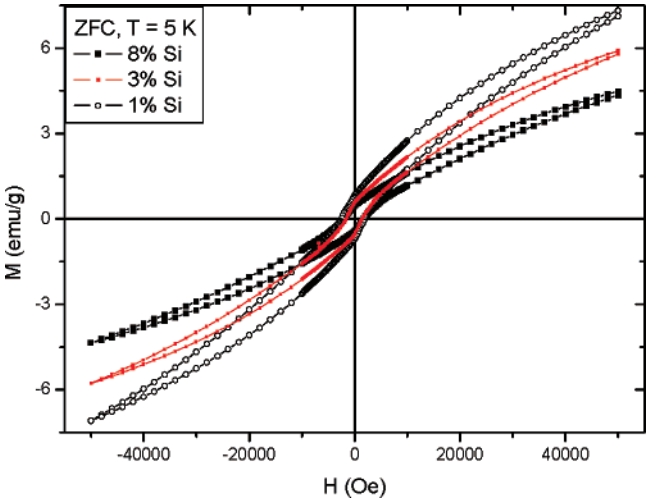

Figure 10. ZFC hysteresis loops recorded at 5 K of ferrihydrites samples containing different amounts of silica.

component is visible in the nonsaturation behavior of the hysteresis loops in fields up to ±50 kOe.

The FC magnetization curves were recorded after the sample was cooled in an applied field of 50 kOe from 300 K (above the blocking temperature, T_B = 70 K, but below the Néel temperature, T_N = 350 K) to 5 K. The FC curve shows a coercivity of 700 Oe, a remanence magnetization of 3.6 emu g^{-1}, and a shift along the field axis of about −300 Oe. Interestingly, we observed that the cooling procedure induces a change in the shape of the hysteresis loop at low temperatures. In comparison to the ZFC magnetization curve, the FC curve approaches saturation much more rapidly, is taller, and has a smaller coercivity (see Figure 8). Moreover, these features of the FC loops vanished at temperatures above 30 K. This is illustrated in Figure 9, where the magnetization curves for three different temperatures are shown. One can see that the shape of the magnetization curves strongly depend on the measured temperature. Below 30 K, the hysteresis loops are narrow for the magnetization close to zero (in the low-field region) and asymmetric. Similar features of the FC magnetization curves of nanoscale ferrihydrite were observed by Punnoose et al. in 5 nm ferrihydrite nanoparticles.[41] These features in the hysteresis loops below 30 K can be explained by assuming that the surface spins exist in a spin-glass-like state.[42] In principle, the basic ingredients for a glassy behavior, such as magnetic frustrations and disorder, are present in our system. The magnetic frustrations are due to the broken symmetry at the particle surface and the presence of competitive magnetic interactions, while the randomness may be created by the distribution of anisotropy axes. There are other features in our magnetic measurements that suggest the existence of a spin-glass-like phase, such as (a) the large irreversibility between ZFC and FC curves in $M(T)$ measurement (Figure 7), (b) the opened loop feature, which is visible in Figure 8 as high-field irreversibility of magnetization on the right-hand side, and (c) the shift of the hysteresis loop along the field axis, which can be explained as arising from the exchange coupling between the AFM ordered core spins and the spin-glass-like surface spins. All of the above findings can be used as fingerprints for the existence of a spin-glass-like behavior.

We are aware that the presence of ferromagnetic impurities can be crucial in experimental studies on AFM nanoparticles. Therefore, we have examined the samples via different characterization methods (EDX and XPS), and within the detection limit, no external magnetic impurities have been identified. In line with our observations and interpretation, recently, similar behavior has been reported for systems of AFM nanoparticles with spin-glass-like surfaces: Co_3O_4,[27] $(Mn,Fe)_2O_{3-t}$,[43] NiO, and α-Fe_2O_3.[44]

Using a particle size of 7 nm, as estimated from TEM investigations, and a density of about 3.8 g cm^{-3} for ferrihydrite, a number of 1.46×10^{18} particles per gram is calculated.

On the basis of the value of the spontaneous magnetization measured at 5 K, M_s = 4 emu g^{-1}, which was found by extrapolation of the linear part (H > 30 kOe) of the high-field magnetization to zero field, an effective magnetic moment per particle of 295 μ_B was estimated. Another estimation of the magnetic moment per particle can be obtained by using the Néel model. Néel suggested that, in a single-domain AFM nanoparticle, N^x spins will remain uncompensated, where N is the total number of atoms in the particle and x can take the value 1/2, 1/3, or 2/3.[25,46] These values depend on how the uncompensated spins are distributed in the crystal lattices, which in turn depends on the crystal structure, particle size, and particle morphology. The uncompensated magnetic moments are given by $\mu_{uc} = \mu_{atom}N^x$, where μ_{atom} is the atomic moment (about 5.9 μ_B for Fe^{3+} ions). Based on this, we obtained uncompensated magnetic moments of about 290, 72, and 1011 μ_B, respectively, depending on the choice of x. An excellent agreement with our measured value was obtained for x = 1/2. According to the Néel model for imperfect sublattice compensation in small AFM nanoparticles, $\mu_{uc} = \mu_{atom}N^{1/2}$ is associated with a random distribution

(41) Punnoose, A.; Phanthavady, T.; Seehra, M. S.; Shah, N.; Huffman, G. P. *Phys. Rev. B* **2004**, *69*, 054425.
(42) Binder, K.; Young, A. P. *Rev. Mod. Phys.* **1986**, *58*, 801.
(43) Passamani, E. C.; Larica, C.; Margues, C.; Takeuchi, A. Y.; Proveti, J. R.; Favre-Nicolin, E. *J. Magn. Magn. Mater.* **2007**, *314*, 21.
(44) Zysler, R. D.; Winkler, E.; Vasquez, Mansilla, M.; Fiorani, D. *Physica B* **2006**, *384*, 277.
(45) Ref deleted in proof.
(46) Richardson, J. T.; Yiagas, D. I.; Turk, B.; Forster, K.; Twigg, M. V. *J. Appl. Phys.* **1991**, *70*, 6977.

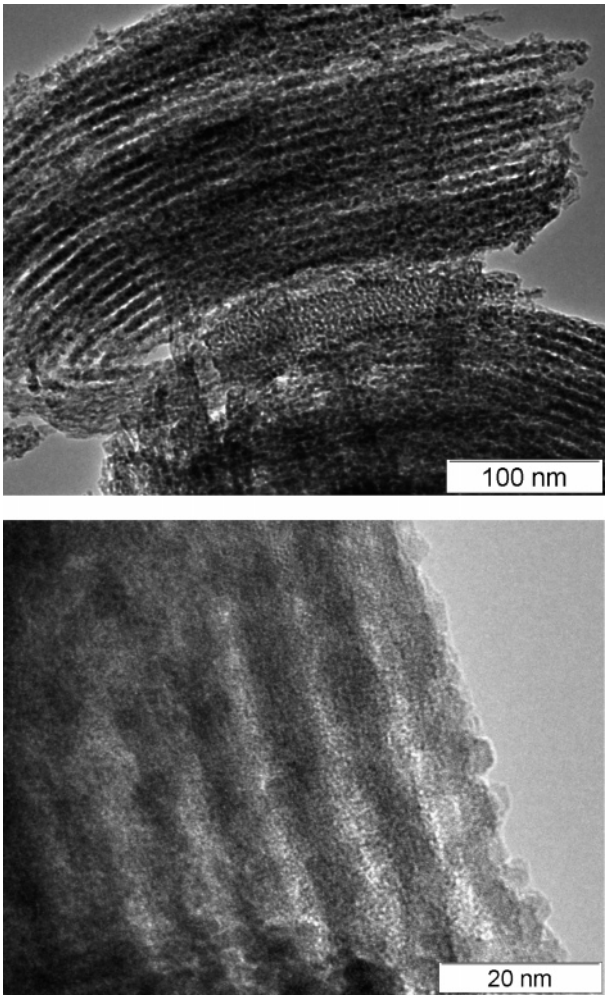

Figure 11. TEM images for mesoporous 2D-ferrihydrite.

of the missing magnetic ions. This is in line with our assumption of a spin-glass-like state at the surface.

Another interesting aspect is the influence of the silica on the magnetic properties. This is shown in Figure 10, where the hysteresis loops for three samples with different silica content are shown. We have observed that a reduction of the amount of silica in the sample leads to increases in coercivity and magnetization. A detailed study of the effect of the silica on the magnetic properties is under investigation.

^{57}Fe Mössbauer spectroscopy was also used to characterize the nanoscale ferrihydrite. The typical Mössbauer spectrum recorded at room temperature is shown in Figure S1 in the Supporting Information. The isomer shift at room temperature, as obtained from fits of the measurement with two lorenzian lines, is 0.34 mm s^{-1}. This indicates that the ferric iron is present in the high-spin state. A value for the quadrupole split of 0.75 was measured. These parameters are characteristic of ferrihydrite.[47,48]

In order to check the versatility of this nanocasting method for the production of nanostructured ferrihydrite, we have also synthesized hexagonal ordered mesoporous two-line ferrihydrite (2D-ferrihydrite) using SBA-15 as a template. The resulting arrays of ferrihydrite nanowires were analyzed with nitrogen physisorption, TEM, and powder XRD. The main results are briefly summarized below. The well-ordered hexagonal mesoporous structure and the poorly crystalline phase of ferrihydrite can be seen clearly from low- and wide-angle XRD patterns (see Supporting Information, Figure S2-A,B). The (100) Bragg reflection at low angles represents the hexagonal ordering of the mesoporous structure, whereas the two broad reflections at higher 2θ values belong to the defective crystal structure of two-line ferrihydrite. The nitrogen adsorption−desorption isotherm (see Figure S3 in the Supporting Information) indicates a type IV isotherm, similar to that of 3D-ferrihyrite. The nanocasted 2D-ferrihydrite has a large surface area of 228 m^2 g^{-1} and a pore volume of 0.39 cm^3 g^{-1}. In the inset, the pore size distribution is plotted. The maximum is located at 5.2 nm. Figure 11 shows the TEM images of hexagonally ordered ferrihydrite. The length of the nanowires varies in the range of 450−1200 nm, and a mean diameter of about 7 nm was extracted from TEM studies (see Supporting Information, Figure S4-A,B, for wider range TEM images of 3D- and 2D-ferrihydrite). Generally, the magnetic properties of hexagonal two-line ferrihydrite are similar to those of the cubic ferrihydrite (data no shown). The ZFC/FC temperature dependence of magnetization reveals the same blocking temperature ($T_B = 70$ K). In contrast to cubic mesoporous nanostructure, for the hexagonal nanowires a very large ZFC coercivity of about 1600 Oe at 5 K was measured. This enhancement of low-temperature coercivity can be attributed, for example, to the magnetostatic dipole interactions between the nanowires or/and is due to contributions from the shape anisotropy. Moreover, coercivity has a strong dependence on the aspect ratio (the length of the wire divided by wire diameter). In our case, a very large aspect ratio (larger than 60) can also lead to this large value for the coercivity.

Conclusions

Hexagonal and cubic ordered mesoporous two-line ferrihydrite samples have been prepared for the first time via the nanocasting pathway. The materials show interesting magnetic behavior with a spin glass state caused by uncompensated spins due to the small structure size. The zero-field-cooled magnetization curve exhibits a peak characterizing a blocking behavior of $T_B = 70$ K. Below the blocking temperature, the particles are ferromagnetic, and an average uncompensated moment of the order of 295 μ_B per particle was estimated. The FC hysteresis curves showed strongly asymmetric hysteresis loops, which are smeared out with increasing temperature. The hexagonally ordered ferrihydrite nanowires yield large low-temperature coercivity up to 1.6 kOe.

The nanocasting route has some crucial advantages for the synthesis of ordered mesoporous iron oxides, and especially ferrihydrite. Due to the unfavorable solution chemistry of iron compounds, direct synthesis via liquid crystal templating is not viable, and in addition, removal of the template often induces redox processes, which are detrimental for highly redox-active elements such as iron. Thus, nanocasting so far remains as the only pathway for the synthesis of an iron oxide polymorph which is difficult to make, such as ferrihydrite. In addition, the size of the structures can be well controlled by the hard templating route, which will prove to be highly important in the construction of future magnetic 3D composites with tailored properties. However, there are also some drawbacks in this

(47) Madsen, M. B.; Mørup, S.; Koch, C. J. W. *Hyperfine Int.* **1986**, *27*, 329.
(48) Guyodo, Y.; Banerjee, S. K.; Penn, R. L.; Burleson, D.; Berquo, T. S.; Seda, T.; Solheid, P. *Phys. Earth Planet. Int.* **2006**, *154*, 222.

synthetic route, such as the additional steps needed, the relatively complex synthesis, and the limited degree of control over the domain size of the magnetic domains so far achieved. Nevertheless, especially the last point is a subject of intensive studies, and it should be at least partially solved by more refined synthetic protocols.

Acknowledgment. We thank A. Göbels for the SQUID, Dr. E. Bill and B. Mienert for the Mössbauer spectroscopy measurements (Max-Planck Institute for Bioinorganic Chemistry, Mülheim an der Ruhr, Germany), and B. Spliethoff for the HRTEM images. We thank F. Radu (BESSY GmbH, Berlin) for fruitful discussions. This work was supported partially by the Leibniz Program of the DFG.

Supporting Information Available: Mössbauer spectrum of cubic ordered ferrihydrite, obtained at 300 K; low- and wide-angle XRD patterns; nitrogen adsorption−desorption isotherms; and pore size distribution for hexagonal ordered mesoporous ferrihydrite. This material is available free of charge via the Internet at http://pubs.acs.org.

JA075528J